Received: 2 November 2023 | Revised: 16 January 2024 | Accepted: 28 January 2024

DOI: 10.1002/agt2.521

Aggregate Open Access WILEY

RESEARCH ARTICLE

3D/4D printed versatile fibre-based wearables for embroidery, AIE-chemosensing, and unidirectional draining

Pengchao Liu[1,2] | **Chengshengze Chu**[1] | **Wenqi Qiu**[3,4] | **Lizi Cheng**[1] | **Jialun Gu**[1] | **Zhengyi Mao**[1,5] | **Zheng Zhao**[8] | **Xinyuan He**[6] | **Guo Liu**[1] | **Chen Peng**[7] | **Kwan Man**[4] | **Ben Zhong Tang**[8] | **Jian Lu**[1,2,5,9]

[1]Department of Mechanical Engineering, City University of Hong Kong, Kowloon, Hong Kong, China

[2]CityU-Shenzhen Futian Research Institute, Shenzhen, China

[3]Department of Plastic and Aesthetic Center, The First Affiliated Hospital, College of Medicine, Zhejiang University, Hangzhou, China

[4]Department of Surgery, School of Clinical Medicine, LKS Faculty of Medicine, The University of Hong Kong, Pokfulam, Hong Kong, China

[5]Centre for Advanced Structural Materials, City University of Hong Kong Shenzhen Research Institute, Greater Bay Joint Division, Shenyang National Laboratory for Materials Science, Shenzhen, China

[6]Department of Chemistry, The Hong Kong University of Science and Technology, Kowloon, Hong Kong, China

[7]Department of Radiology, Shanghai Public Health Clinical Center, Fudan University, Shanghai, China

[8]School of Science and Engineering, Shenzhen Institute of Aggregate Science and Technology, The Chinese University of Hong Kong, Shenzhen, Guangdong, China

[9]Laboratory of Nanomaterials and Nanomechanics, City University of Hong Kong, Hong Kong, China

Correspondence
Prof. Chen Peng, Department of Radiology, Shanghai Public Health Clinical Center, Fudan University, Shanghai 201508, China.
Email: cpengrr@tongji.edu.cn

Prof. Ben Zhong Tang, School of Science and Engineering, Shenzhen Institute of Aggregate Science and Technology, The Chinese University of Hong Kong, Shenzhen, Guangdong 518172, China.
Email: tangbenz@cuhk.edu.cn

Prof. Jian Lu, Department of Mechanical Engineering, City University of Hong Kong, Kowloon, Hong Kong, China.
Email: jian.lu@cityu.edu.hk

Funding information
Shenzhen-Hong Kong Science and Technology Innovation Cooperation Zone Shenzhen Park Project, Grant/Award Number: HZQB-KCZYB-2020030; Hong Kong RGC Theme-based Research Scheme, Grant/Award Number: AoE/M-402/20; Shenzhen Science and Technology Program, Grant/Award Number: JCYJ20220818101204010

Abstract

Fibre-based wearables for embroidery, chemosensing, and biofluid's unidirectional draining with good flexibility, tunability, and designability drive technological advance. However, synthetic polymer fibres are non-degradable, threatening the environment and human health. Herein, we have developed versatile microfibre-based wearables by combining many advantages in one platform of biodegradable polylactic acid (PLA) and melt electrowriting strategy. Diverse potential applications of PLA wearables are achieved by flexibly designing their printing files, components and structures. Three-dimensional printing files are generated from two-dimensional images to fabricate 'embroidery-like' patterns. PLA/aggregation-induced emission fluorogens (AIE) chemosensors exhibit colorimetric and fluorescent colour changes upon exposure to amine vapours. Janus PLA-cotton textiles with a hydrophobic/hydrophilic structure could facilitate unidirectional draining of sweats which is favourable for the management of temperature and humidity on the surface of skin. The proposed platform can not only broaden the design possibilities in 3D/4D printing but also offer wide potential applications for functional wearables.

KEYWORDS
3D/4D printing, aggregation-induced emission, chemosensing, fibre-based wearable, polylactic acid, unidirectional draining

1 | INTRODUCTION

Fibre-based assemblies (i.e. fibres, yarns, and fabrics/textiles) are promising support materials for the next generation of functional wearables, with applications spanning display technologies,[1] health monitoring,[2,3] stealth operations,[4] and energy harvesting/storing,[5,6] given their low weight, flexibility, deformability, breathability, and design adaptability.[7] However, synthetic polymers, such as polyethylene terephthalate, polypropylene, polyvinyl chloride, polyethylene, and polyurethane, derived from petroleum, are typically used to prepare fibres. Owing to the

non-degradable nature of synthetic polymers and inadequate waste management, their use has led to the emergence of environmental pollution as a long-term problem, affecting the biosphere and human health worldwide.[8] The accumulation of synthetic polymer particles (i.e., micro/nano-plastics[9]) in the organs of animals may result in liver damage, neurotoxicity, and inflammatory responses.[10] Furthermore, nano-plastics have been detected in human blood,[11] with adverse effects observed in the offspring of adult mice.[12] To address this severe problem and 'close the loop' on plastics, it is necessary to explore the use of degradable or recyclable materials for fibre-based wearables.

Naturally derived materials, such as gelatine, poly-hydroxy butyrate-*co*-valerate, poly-hydroxy butyrate, and PLA, have emerged as promising substitutes for the preparation of fibre-based assemblies owing to their degradability.[13] PLA, in particular, is renewable and biodegradable as it is derived from agricultural products, such as corn or other carbohydrate sources. Consequently, PLA has been applied in packaging, transportation, agriculture, textiles, and high-value-added biomedical industries such as sutures,[14] bone screws, orthopaedic implants,[15] and tissue engineering scaffolds.[16] The degradability of PLA occurs in several ways, including hydrolytic,[17] oxidative,[18] thermal, microbial, enzymatic,[19] chemical and photo degradation.[20] As a result, these degradative methods cause PLA main and side chains to undergo scissions, even complete decomposition into carbon dioxide and water.[21] From the view of environmental protection and human health, the desired degradability of PLA is complete decomposition. Moreover, PLA exhibits piezoelectric properties,[22,23] high mechanical strength, and considerable stiffness, rendering it a favourable candidate for fused deposition modelling (FDM) three-dimensional (3D) printing. PLA filaments can be extruded from the nozzles of FDM machines and deposited layer-by-layer for constructing the target architectures. However, the printing resolution for FDM is extremely low (>100 μm),[24] which limits the flexibility of PLA fibre-based wearables, rendering them uncomfortable to wear, especially on uneven skin surfaces. An alternative manufacturing method for PLA fibres is melt/solution electrospinning, which results in the deposition of nanofibres with dense structures. However, it is challenging to precisely control the network architecture of PLA fibres during electrospinning processes. Thus, both FDM 3D printing and electrospinning present limitations for the preparation of PLA fibre-based wearables.

Melt electrowriting (MEW),[25] a special 3D printing strategy based on melt electrospinning, can enable the direct writing (DW) of microfibres with diameters as small as 0.8 μm.[26] This advanced strategy combines the high printing resolution of electrospinning with the precise structural control offered by 3D printing and is thus promising for preparing fibrous structures. Since the development of MEW by Paul's group in 2011,[27] poly(ε-caprolactone) has remained the gold-standard polymer for MEW applications. However, poly(ε-caprolactone) has a long degradation time, and thus, it is necessary to identify degradable materials, such as PLA, for use in MEW frameworks. Research on the integration of PLA and MEW technology remains scarce. The existing studies[28–30] have mainly focused on the preparation and characterisation of PLA lattices, with limited exploration of their practical applications, such as functional wearables.

Therefore, in this study, by integrating PLA and MEW strategy, we developed PLA microfibre-based wearables with diverse functionalities such as the realisation of embroidery-like patterns, chemosensing, and unidirectional draining of biofluids (the schematic of the design shown in Figure 1). Due to their degradable properties, PLA fibre-based wearables are suitable for temporary applications or frequently renewed devices. To this end, the following steps were implemented: conversion of two-dimensional (2D) images to 3D models for generating the printing files of PLA patterns, componential design by doping AIE particles within the PLA matrix for chemosensing, and the structural design of Janus PLA-cotton (JPct) hydrophobic/hydrophilic constructs to enable the unidirectional draining of biofluids. The proposed platform can be applied in varied application scenarios through appropriate componential and structural design. The combination of naturally derived materials and a 3D printing strategy can expand the design possibilities in the four-dimensional (4D) printing domain and extend the range of potential applications of functional wearables.

2 | RESULTS AND DISCUSSION

2.1 | Fabrication of PLA microfibres and meshes

The fabrication of fibre-based wearables is based on the hierarchical assembly of fibrous materials, such as one-dimensional fibres and yarns, 2D mesh/fabric structures, and 3D spacer fabrics/textiles.[7] In this study, PLA microfibres and meshes were successfully fabricated using the MEW strategy. Figure 2A shows the MEW unit used in our 3D bioprinting equipment. The unit has two separate temperature-controllable zones: a cartridge zone with a temperature of 150°C (Heat 1) for the temporary storage of PLA powder; and a nozzle zone with a temperature of 190–220°C (Heat 2), comparable to or exceeding the melting point of PLA. This dual temperature-controllable setup can mitigate the degradation of PLA at high temperatures. The MEW process involves many parameters,[26,27,31] with the key parameters for the printing of PLA including the printing speed and nozzle temperature, which define the stretchability and viscosity of polymer melt, respectively. Starting with the case where the nozzle's temperature was fixed at 190°C, PLA filaments were written at different printing speeds. Figure 2B shows the PLA microfibre morphologies: At printing speeds of 200, 150, 100–75, and 50–25 mm/s, the PLA microfibres were written in straight lines, sinusoidal waves, "0-shaped" curves, and "8-shaped" curves, respectively. The effect of the nozzle temperature on the morphologies of PLA microfibres is illustrated in Figure S1. As the printing temperature increased from 190 to 220°C, PLA microfibres appeared in straight-line, sinusoidal wave, "0-shaped" curve, and random coil morphologies. Using the proposed system, PLA microfibres in straight-line configuration were obtained at a nozzle temperature of 190°C and a printing speed of 200 mm/s, appropriate for the fabrication of PLA meshes and patterns.

Next, PLA meshes were fabricated using the straight-line configuration obtained at different printing angles (i.e., 45°, 60°, and 90°, Figure 2C) and unit cell widths (800 μm, Figure 2C; 400, 200, and 100 μm, Figure 2D). The average

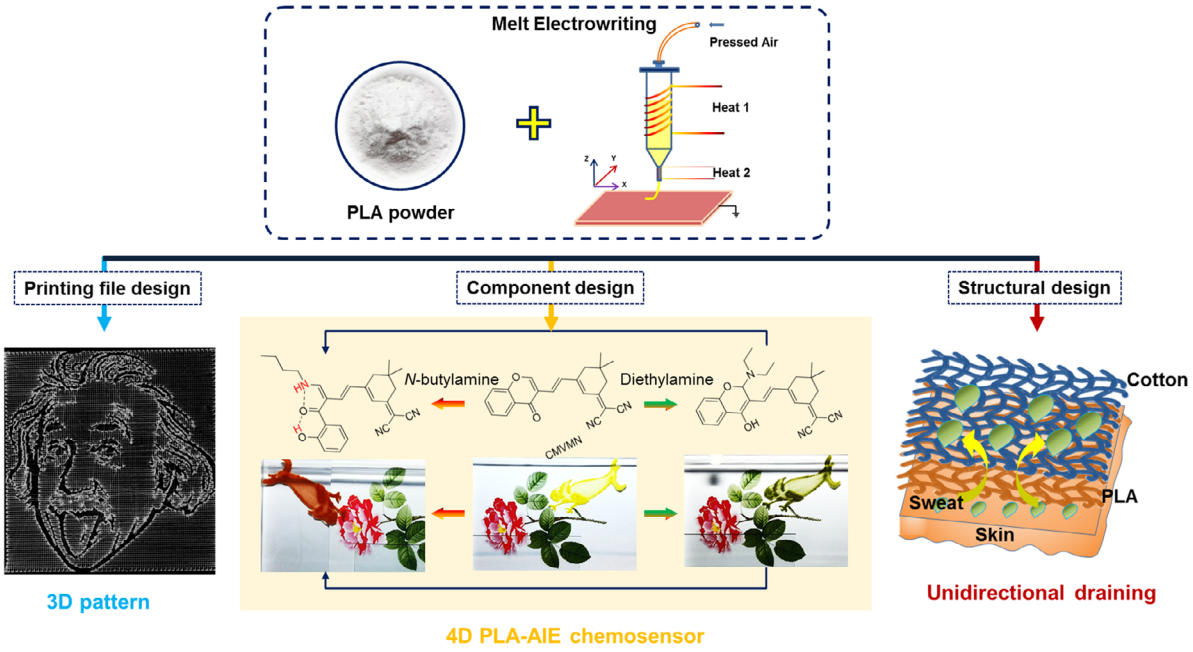

FIGURE 1 Schematic diagram showing the designs of versatile PLA microfibre-based wearables based on a proposed platform of PLA biopolymer and MEW strategy.

diameter of the PLA microfibres was ≈27 μm. When the unit cell width was 100 μm, electrostatic interactions[32,33] among the fibres led to deviations from the intended path for PLA fibre deposition. The effects of the voltage and printing speed on the morphologies of the PLA microfibre-based meshes are shown in Figures S2 and S3, respectively. The largest PLA mesh obtained using the 3D bioprinting platform exhibited dimensions of 21 cm (length) × 14 cm (width) (Figure 2E). The prepared PLA meshes exhibited diverse processing possibilities (tailoring, origami, and rolling (Figure 2E)) and good biocompatibility (Figure S4), demonstrating the suitability of PLA as the matrix material for fibre-based wearables. Figure 2F-H illustrate the potential applications of PLA microfibre-based wearables, i.e. embroidery, chemosensing, and unidirectional draining. PLA was 3D printed into a "City U" pattern, highlighting its applicability for preparing industrial logos (Figure 2F). Additionally, a 4D-printed PLA-AIE chameleon-like sensor exhibited visible colour changes upon exposure to chemical vapours (Figure 2G). By printing PLA mesh onto a cotton collector, a JPct with unidirectional draining ability was obtained, which could facilitate humidity and temperature management of human skin (Figure 2H).

2.2 | Generation of printing files for PLA patterns

The printing files for PLA patterns were generated using the boundary effect and the conversion of 2D images to 3D models. The boundary effect was observed in the MEW process. For example, in the case of a square-shaped sample (Figure 3A), the obtained PLA mesh could be divided into four zones from the centre to the periphery: the DW zone and zones I, II, and III. In zones I, II, and III, the PLA fibres appeared as random coils. Moreover, intensified tangling of PLA microfibres was observed close to the boundaries, attributable to the gradual reduction in printing speed from DW to zone III. This phenomenon was termed the boundary effect.

Moreover, 2D images were converted to printable 3D models using *3D Builder* (20.0.4.0, Microsoft Corporation), a software pre-installed on Microsoft Windows 10. A lotus-shaped PLA pattern was prepared to illustrate the generation of printing files based on the boundary effect and the conversion of 2D images to 3D models. In route 1, the 2D lotus image was processed only using *3D Builder*, resulting in the formation of only the external contour of the lotus. In contrast, in route 2, we constructed the boundaries (black lines in the 2D image, Figure 3B) for the lotus before generating the printing G-code using *3D Builder*, leading to a regionalization of the entire printing pattern. Therefore, vivid structures of a lotus pattern with more details were achieved. Compared with route 1 (2D-image-to-3D model only), route 2 (boundary effect + 2D-image-to-3D models) appeared superior for the generation of printing files of PLA patterns. Consequently, all the printing files of PLA patterns were generated according to route 2 in the following experiments.

2.3 | 3D-printed embroidery-like patterns: Merging art and technology

PLA embroidery-like patterns were fabricated using the MEW strategy for decorative applications, representing a fusion of embroidery art and 3D printing technology. Motifs such as plum blossom, orchid, bamboo, and peony, which are revered owing to their positive connotations of fortitude, elegance, modesty, and wealth, respectively, have served as prototypes for traditional embroidery. To generate files for the 3D printing of embroidery-like PLA patterns, the 2D images of these four plants and one famous Tang poem (Figure 4A) were processed. Figure 4a shows the written structures, characterised by two layers of PLA microfibres (tetragonal unit

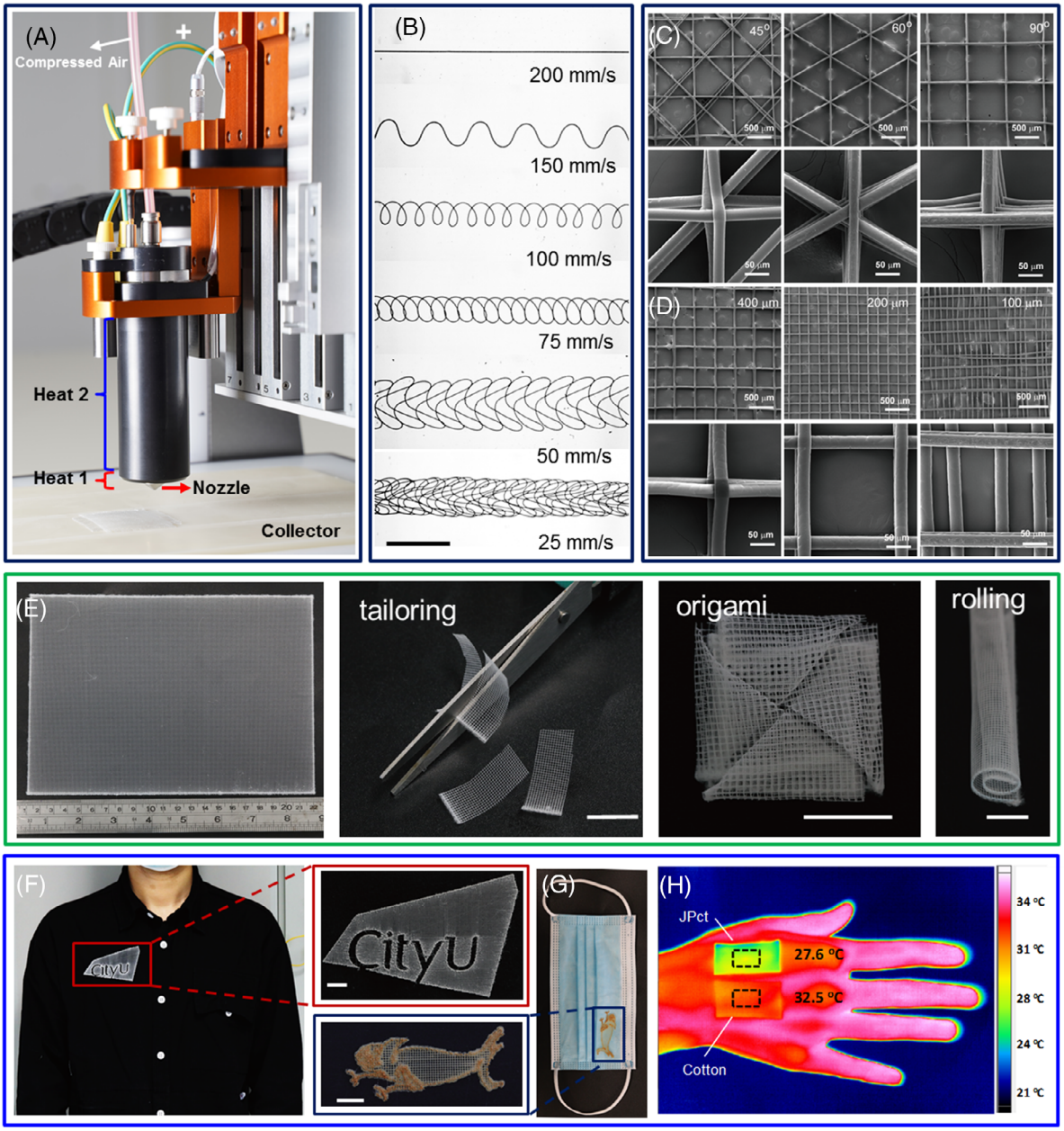

FIGURE 2 Fabrication and characterisation of PLA microfibre-based assemblies. (A) Photograph of the MEW unit for PLA microfibre-based assemblies in our bioprinting equipment. (B) Photographs of PLA microfibres prepared at different writing speeds (scale bar: 1 mm). (C) SEM images of PLA meshes with straight microfibres at writing angles of 45°, 60°, and 90° (unit cell width: 800 μm). (D) SEM images of PLA meshes with unit cell widths of 400, 200, and 100 μm. For (B–D), the same parameters were used: nozzle temperature of 190°C, extrusion pressure of 30 kPa, and voltage of 5 kV. (E) Photographs of PLA mesh sized 21 cm (length) × 14 cm (width) and its versatile operation in tailoring, origami, and rolling. (F) 3D-printed "CityU" logo. (G) 4D-printed chameleon-shaped pattern with visually observable colour-changing ability for chemosensing. (H) 3D-printed JPct with unidirectional draining ability for temperature management. The scale bar in (E–H) is 1 cm.

cells) with a thickness of approximately 54 μm. Through a similar process, 2D images of the logo of the Barcelona football team, a portrait of Albert Einstein, the logo of the City University of Hong Kong, and a painting by Pablo Picasso (Figure 4B-E, respectively) were processed and printed by MEW. The corresponding photographs of the 3D-printed PLA patterns are presented in Figure 4b-e.

2.4 | 4D-Printed PLA-AIE chemosensors

As discussed, PLA microfibre-based meshes can be written in different patterns. Based on this capability, we explored the potential application of these meshes as functional fibre-based wearables by appropriately designing the components and structures.

AIE fluorogens, first reported in 2001,[34] are materials that exhibit intensified fluorescence in the aggregate or solid state. AIE particles can be doped within the matrices of polymer fibres[35,36] and hydrogels[37,38] for preparing optoelectronic devices, fluorescent sensors, and biomedical probes.[39–41] From the perspective of component design, we prepared PLA-AIE chemosensors with visually observable colour-changing abilities, representing a unique facet of 4D printing. Notably, (*E*)−2-{5,5-dimethyl-3-[2-(4-oxo-4*H*-chromen-3-yl)vinyl]cyclohex-2-en-1-ylidene}malononitrile (abbreviated as CMVMN, Figure 5A) is a chromone-based AIE luminogen with selective amine-identification

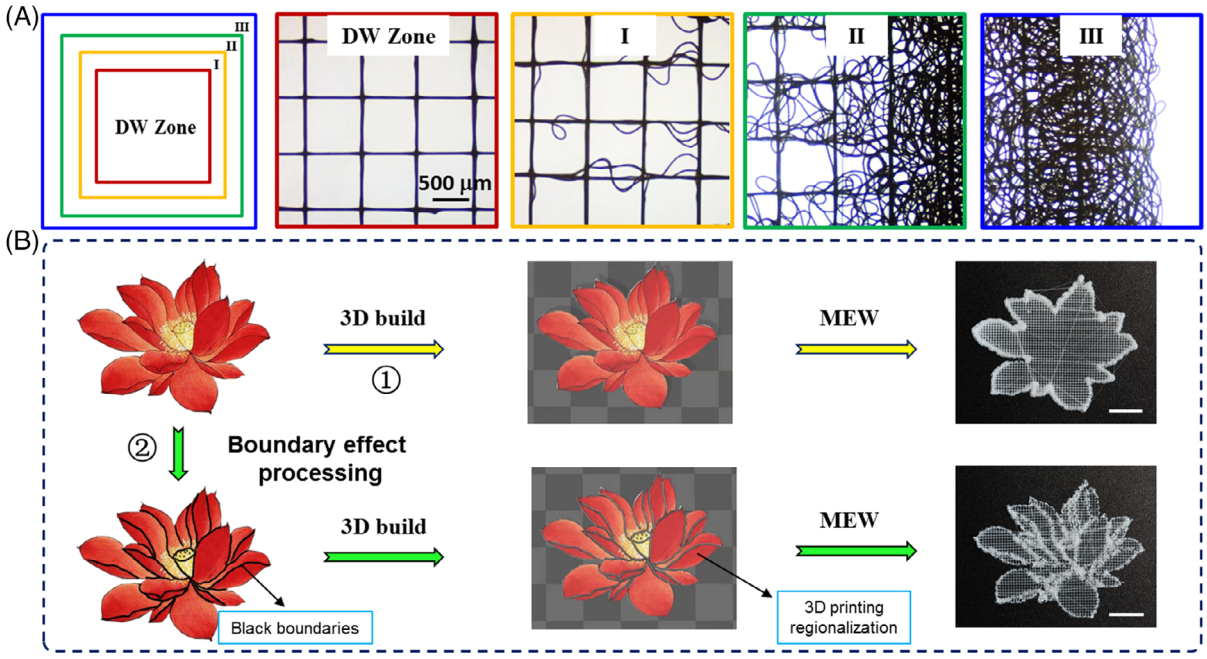

FIGURE 3 Printing file generation for PLA patterns. (A) Schematic of boundary effect and photographs of PLA microfibres in different regions of the PLA mesh. Straight PLA microfibres were obtained only in the central DW zone, while random coils were observed in zones I, II, and III. (B) Comparison of two process routes for printing files of PLA lotus-shaped pattern from 2D lotus image: route 1: 2D-image-to-3D models only; route 2: boundary effect + 2D-image-to-3D models strategy. Scale bar: 1 cm.

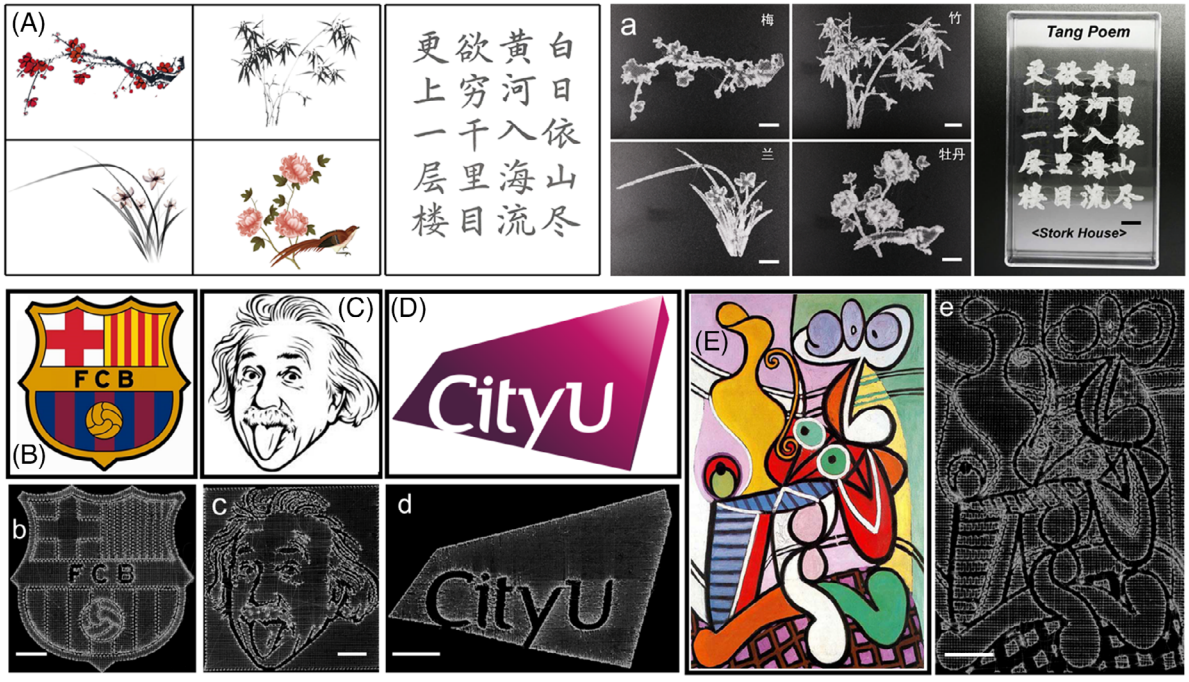

FIGURE 4 3D-printed PLA patterns. (A) Pictures of Chinese traditional paintings and an ancient poem. (B) Logo of the Barcelona football team. (C) Portrait of Einstein. (D) "CityU" logo of the City University of Hong Kong. (E) Painting by Pablo Picasso. (A–E) Corresponding printed patterns of (A–E). Scale bar: 1 cm.

capacities, as demonstrated in our previous work.[42] Specifically, CMVMN reacts with primary and secondary amines to present different colours under UV light and white light. Thus, in this study, PLA and CMVMN powders were mixed and melted homogeneously for preparing "maple leaf" and "chameleon" sensors. *N*-butylamine and diethylamine were chosen as the models of primary and secondary amines, respectively, to induce colour changes in the PLA-CMVMN chemosensor. Figure 5A shows the reactivities of CMVMN towards *N*-butylamine and diethylamine.

CMVMN particles are functionally sensing components in the PLA-AIE chemosensor. From our previous study,[42] CMVMN showed high thermostability (thermal decomposition temperature: 294°C). For its sensing response, we

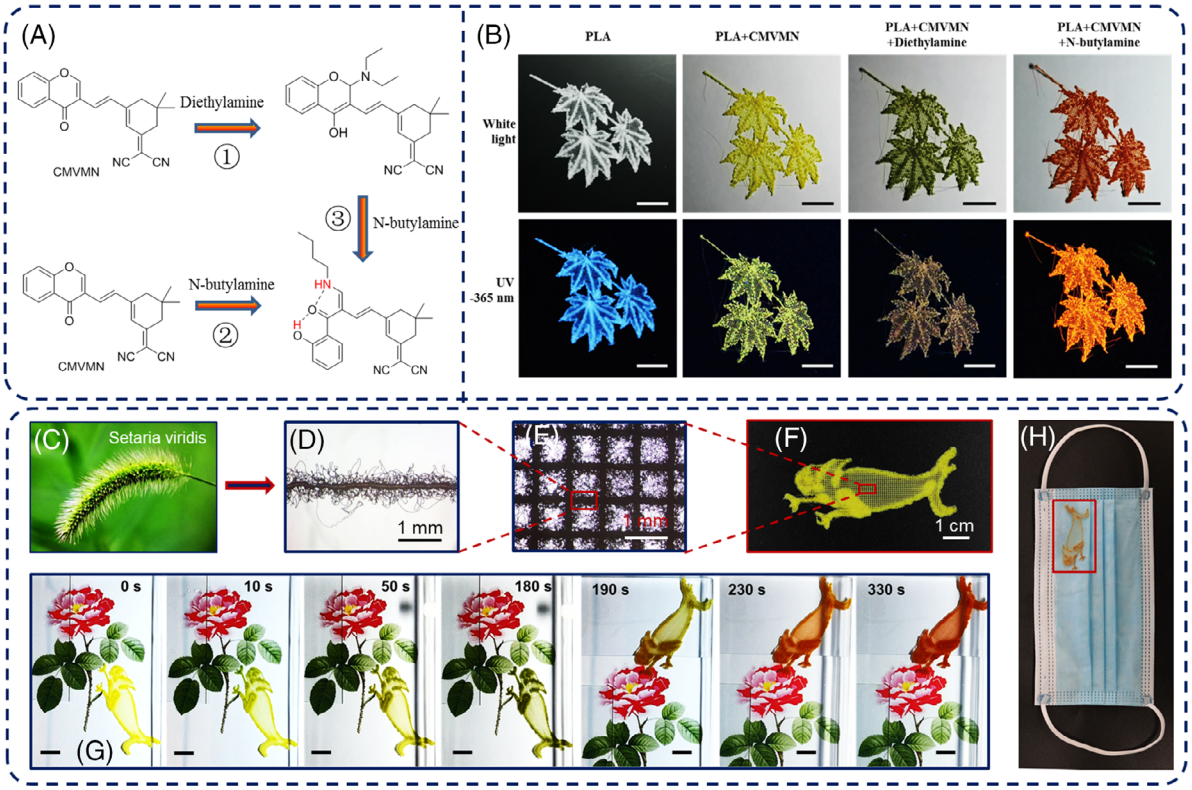

FIGURE 5 PLA-AIE sensor with visually colour-changing ability. (A) Chemical reactions between CMVMN and amines (*N*-butylamine and diethylamine, chosen as primary and secondary amine models, respectively). The reaction mechanism[42] of CMVMN with amines is a kind of nucleophilic addition, which causes the amination and bioconjugation of CMVMN with secondary amine (i.e. diethylamine, ①) and primary amines (i.e. *N*-butylamine, ②). The reactivity and fluorescent sensing response of CMVMN towards amines is related to the steric effect of amines. *N*-butylamine is with weaker steric effect than diethylamine. Under the same conditions, *N*-butylamine shows higher reactivity and selectivity of CMVMN than diethylamine (③). (B) Optical photographs of PLA, PLA-CMVMN, PLA-CMVMN (diethylamine vapour), and PLA-CMVMN (*N*-butylamine vapour) maple leaf-shaped sensors under white light and UV light (λ = 365 nm). Optical photographs of (C) *Setaria viridis*, (D) a single PLA fibre with biomimetic structure, (E) a PLA-CMVMN mesh, and (F) a PLA-CMVMN chameleon-shaped sensor. (G) Optical photographs of the continuous colour-changing process of PLA-CMVMN chameleon-shaped sensor at different time intervals (0–180 s: diethylamine vapour, 190–330 s: *N*-butylamine vapour). (H) Optical photograph of a chameleon-shaped sensor on a mask, illustrating a potential application scenario.

have proven that CMVMN exhibited good stability after repeated exposure to the same amine vapours, as evidenced by the similar spectrum to that of the initial sample from the ^{1}H NMR[42] measurement. Its fluorescence keeps almost constant and such stability is favourable for sensing. The maple leaf-shaped chemosensor exhibited colorimetric and fluorescent dual-mode abilities for detecting amine vapours, as shown in Figure 5B. As a control sample, a neat PLA maple leaf exhibited white and blue colours under white light and UV light, respectively. Under white light, the PLA-CMVMN maple leaf appeared bright yellow, which transitioned to dark green and brick-red colours when in contact with diethylamine and *N*-butylamine vapours, respectively (Movies S1 and S2). Under UV light (λ = 365 nm), the PLA-CMVMN maple leaf appeared light yellow, which transitioned to light pink and tangerine colours by contacting with diethylamine and *N*-butylamine vapours, respectively.

We have found that CMVMN exhibits higher reactivity and selectivity towards primary amines than secondary amines in our previous work.[42] This is because primary amines have a weaker steric effect than secondary amines. The different selectivity of CMVMN to primary and secondary amines was illustrated by the chameleon-shaped chemosensor with continuous colour-changing ability. Owing to a weaker steric effect, the reaction between CMVMN and primary amines is more stable and selective than that between CMVMN and secondary amines[42] (Figure 5A). PLA-CMVMN single fibres were written into a biomimetic structure mimicking *Setaria viridis* (Figure 5C).[43,44] This special multiscale stalk–bristle structure (Figure 5D) was obtained with a printing speed of 50 mm/s at a nozzle temperature of 240°C. At this temperature, the viscosity of the PLA-CMVMN melt was considerably lower than at 190°C, resulting in the ejection speed of the PLA-CMVMN melt exceeding the printing speed. Figure S5 shows photographs of the single PLA-CMVMN microfibres written with printing speeds of 25–200 mm/s at a nozzle temperature of 240°C. These biomimetic fibres, when assembled at angles of 90° (Figure 5E), were ultimately deposited into a chameleon-shaped pattern (Figure 5F) with chemosensing ability.

The chameleon-shaped chemosensor exhibited a continuous colour-change response when placed on a sheet of A4 paper bearing printed images of a red flower and green leaves under white-light illumination (Figure 5G and Movie S3). In the presence of diethylamine, the chameleon-shaped chemosensor transitioned from bright yellow to dark green over 0–180 s. Upon the introduction of *N*-butylamine, the chameleon-shaped chemosensor turned brick-red over 190–330 s. This PLA-AIE fibre-based wearable, based on componential design, can be used as a chemosensor

integrated into masks (Figure 5H) and other personal protective equipment.

2.5 | JPct for unidirectional draining

Cotton textiles are ubiquitously used as clothing or biomedical gauze materials in daily life. However, their thermal- and humidity-regulation abilities are limited, because cotton tends to be wetted by the undifferentiated infiltration of bodily fluids, such as sweat, blood, urine, and other interstitial fluids. For example, excessive sweat may lead to undesired adhesion and a sensation of coldness. Moreover, the presence of biofluid around wounds may result in infections, thereby hindering the healing process.

To address these challenges, we prepared JPct with a hydrophobic/hydrophilic bilayered structure. This construct was achieved by the DW of a hydrophobic PLA microfibre mesh onto hydrophilic cotton textile. To demonstrate its practical application, JPct was placed with the hydrophobic PLA layer close to human skin (Figure 6A). Figure 6B shows the typical bilayered structure of JPct, in which the PLA microfibres form an open cellular structure that can facilitate the transportation of biofluids. Cotton microfibres, with an average diameter of 18.1 ± 4.8 μm (Figure 6C-E), served as a supporting layer and exerted a draining force on the biofluids. In contrast, the PLA microfibre, with an average diameter of 21.1 ± 1.1 μm (Figure 6F-H), constituted a separate layer to prevent biofluid wetting. This JPct, designed from the perspective of structure, can enable the unidirectional drainage of sweat and other biofluids from the skin.

To demonstrate the unidirectional draining ability of the JPct, we used a simplified physical model in which continuous fluorescent-water droplets were extruded from a syringe to mimic excessive sweat or biofluids. We recorded and analysed the dynamic draining process of a green aqueous solution (with 0.1% sodium fluorescein) on JPct under UV radiation ($\lambda = 365$ nm). Neat PLA microfibre mesh and cotton textile were chosen as the controls, as shown in Figure 6I,J. Movies S4 and S5 showed the dynamic contacting and wetting process of fluorescent water droplets to the neat PLA microfibre mesh and cotton textile, respectively. The droplets failed to penetrate and wet the neat PLA microfibre mesh (Figure 6I and Movie S4). However, when the droplet came into contact with the cotton textile, it rapidly penetrated and wetted both sides of the cotton textiles within a short contact time (<3 fs, 30 fs = 1 s). Notably, both the contacting side (top) and reverse side (down) exhibited similar green patterns and fluorescence intensity (Figure 6J and Movie S5).

For the JPct, the droplet of aqueous solution was pumped through its hydrophobic PLA layer and wetted its hydrophilic cotton layer, even if the droplet initially touched the hydrophobic layer directly from above (Figure 6K and Movie S6). Similarly, when the droplet contacted the hydrophobic layer from beneath, it could also penetrate the hydrophobic layer and wet the hydrophilic layer (Figure 6L and Movie S7). Consequently, the hydrophilic layer exhibited a much clearer pattern with higher fluorescence intensity than the hydrophobic layer. These results suggest that the JPct can unidirectionally drain fluids. Furthermore, the JPct exhibited anti-gravity unidirectional draining capabilities (Figure 6L), which can enhance its range of applications, including wound dressings, masks, and insulated mats.

JPct with unidirectional draining ability was used to test its potential application for humidity and temperature management near the skin. Cotton textiles, commonly used as clothing materials, became wet easily by adsorbing sweat. Wetted cotton adheres to the skin owing to the hydrophilicity of the cellulose fibres, which could result in discomfort. In contrast, skin covered with JPct rapidly dried due to the unidirectional drainage of water away from the human skin, resulting in minimal adherence to the skin (Figure 6M). An infrared camera was used to capture images of the skin in both dry and wet states (Figure 6N). In the dry state without sweating, the temperature (31.1°C) of the area covered by the cotton textile was higher than that (29.2°C) of the area covered by the JPct. In other words, JPct exhibited superior heat-insulation properties compared with the cotton textile. In the wet state, induced by sweating, the temperature (26.4°C) of the area covered by JPct was considerably lower than that (30.0°C) of the area covered by the cotton textile. These results highlight that the JPct exhibits enhanced heat insulation (lower thermal conductivity) compared with the cotton textile in both dry and wet conditions. Therefore, the JPct offers a more comfortable sensation with minimal wet adhesion and better heat insulation, especially in scenarios involving perspiration, compared with traditional cotton clothing.

3 | CONCLUSIONS

In summary, by integrating degradable PLA biopolymer and the MEW strategy, PLA microfibres and meshes were produced with varied operability, such as tailoring, folding, and rolling. Possible applications ranging from logo display, chemosensing, and unidirectional draining of biofluids were demonstrated based on our platform. We generated 3D printing files for obtaining PLA embroidery-like patterns by leveraging the boundary effect phenomenon in the MEW and conversion of 2D images to 3D models. Furthermore, PLA-AIE microfibre-based sensors were designed to exhibit colour-changing responses for chemical vapour detection. JPct frameworks with a hydrophobic/hydrophilic structure could realise unidirectional draining of biofluids, thereby facilitating humidity and temperature management. Our findings can promote the advancement of 4D printing and the development of advanced fibre-based wearables with diverse applications.

4 | EXPERIMENTAL SECTION

4.1 | Materials

PLA powder (NatureWorks 4032D) was purchased from Shunjie Plastic Technology Co. Ltd. CMVMN particles were obtained from Prof. Ben Zhong Tang's group. The synthesis and characterization were conducted as previously reported.[42] Diethylamine, *N*-butylamine, and sodium fluorescein were purchased from Sinopharm Chemical Reagent (China).

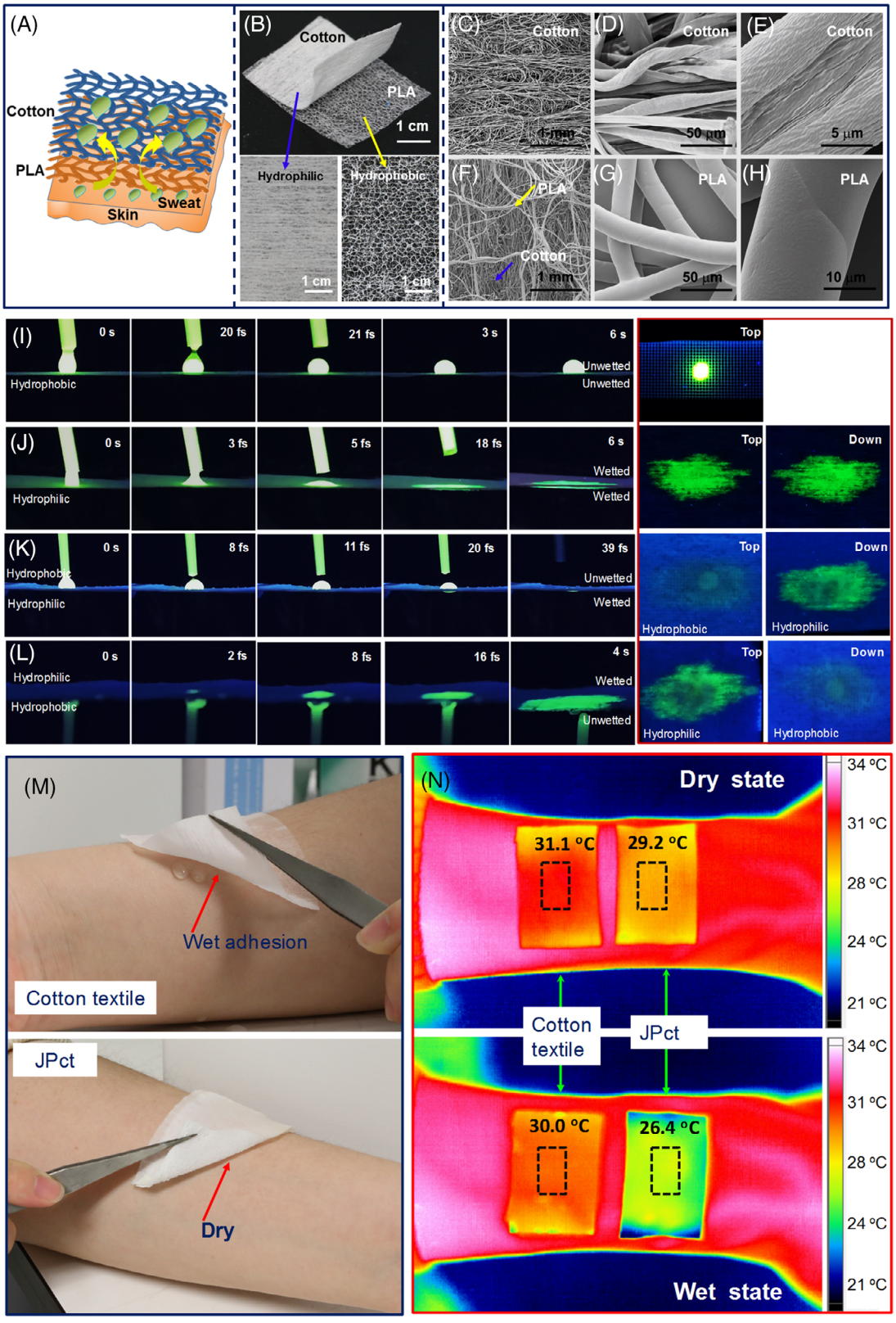

FIGURE 6 JPct for unidirectional draining. (A) Schematic of application scenario of the JPct. (B) Optical images of the bilayered structure of JPct: hydrophilic cotton textile and hydrophobic PLA porous mesh. (C–E) SEM images of cotton textile at different magnifications. (F) SEM image of PLA microfibre in the JPct. (G,H) PLA microfibre in the JPct at different magnifications. Demonstration of unidirectional fluid draining capability of the JPct in comparison with cotton textile. Control experiments: contacting and wetting processes of aqueous solution (0.1% sodium fluorescein, UV radiation [$\lambda = 365$ nm]) for the (I) hydrophobic PLA mesh and (J) hydrophilic cotton textile. The aqueous solution cannot wet the PLA mesh but can penetrate the cotton textile and wet both sides of the cotton textile. (K,L) Contacting and wetting processes of aqueous solution to the JPct from the hydrophobic side to the hydrophilic side. Regardless of the direction of contact, water can penetrate the hydrophobic layer and wet the hydrophilic layer. (M) Optical photographs of cotton and JPct to illustrate water adsorption and transportation. (N) Infrared camera images of the cotton textile and JPct placed on dry and wetted skin.

4.2 | 2D image-to-3D printing files

The 3D printing files were generated from 2D images (i.e., a lotus, a Tang poem, a portrait of Einstein, a painting by Pablo Picasso, a maple leaf, a chameleon, and the logos of Barcelona and CityU) using *3D Builder*, a software pre-installed in Microsoft Windows 10.

4.3 | Fabrication of PLA meshes by MEW

PLA microfibre-based meshes were designed and fabricated using a MEW unit integrated with a bioprinting platform (GeSiM Bioscaffolder 5.1, Grosserkmannsdorf, Germany). Before writing, the PLA powders were dried at 85°C in the oven for 2 h. The dried PLA powders were placed in stainless cartridges (Heat 1 zone in Figure 2A) connected to a stainless nozzle (inner diameter of 250 μm; Heat 2 zone in Figure 2A) for 1 h to form a homogeneous polymer melt. In the DW mode, the distance between the nozzle and collector, the height between two adjacent layers, and the voltage were set as 7.5 mm, 0.01 mm, and 5 kV, respectively. Driven by compressed air with a pressure of 30 kPa, the PLA filaments were extruded from the nozzle and deposited onto a plastic collector at a writing speed of 50–200 mm/s and a nozzle temperature of 190–220°C. Subsequently, the PLA meshes were extracted for characterisation.

4.4 | Fabrication of PLA-AIE maple leaf- and chameleon-shaped chemosensors by MEW

CMVMN crystals were ground into a powder using an agate mortar. The PLA powder (300 mesh) was then thoroughly mixed with the CMVMN powder (1 wt% of PLA). The MEW process for PLA-AIE patterns was similar to that for pure PLA printing. Briefly, the mixture of PLA and CMVMN powders was placed in stainless cartridges (150°C) connected to a stainless nozzle (I.D. 250 μm, 190°C) for writing. The DW speed of the nozzle was 200 mm/s, and the other writing parameters for the maple leaf and chameleon patterns were identical to those in the PLA DW process. Eventually, the maple leaf (60 mm × 47 mm, two-layered height) and chameleon (50 mm × 23 mm, two-layered height) were obtained for further use.

4.5 | Investigation of the colour-changing ability of PLA-AIE maple leaf- and chameleon-shaped chemosensors

The colour-changing processes of PLA-AIE chemosensors was observed under UV–white light (WFH-203C, Shanghai Jingke Scientific Instrument Co., Ltd, China). The maple leaf-shaped chemosensor was placed in a transparent polystyrene rectangular box (12.8 cm × 7.7 cm × 2.0 cm), which was then positioned on the floor in the middle of the UV–white light device. A drop of diethylamine, or *N*-butylamine was introduced in one corner of the box, without contacting the chemosensors, and then the lid of the box was closed. The colour-changing process was documented through photographs captured from a window on the top of the UV–white light device.

4.6 | Fabrication of JPct

The cotton textile was laid flat, with its edges adhering to the plastic collector. The PLA microfibre-based mesh was directly printed onto the cotton textile. JPct was obtained after a certain writing duration.

4.7 | Investigation of the unidirectional water draining ability of JPct through a simplified physical model

A syringe, placed above/under the JPct, continuously supplied fluorescence-labelled water (0.1% sodium fluorescein) at a constant speed. The unidirectional water drainage process was recorded using a digital camera (60D, Canon) under UV radiation ($\lambda = 365$ nm).

4.8 | Characterisation

Optical photographs of the PLA microfibres and meshes prepared by MEW were captured using an optical microscope (Nikon, Eclipse TS100) and environmental SEM (FEI Quanta 250). The diameters of the PCL microfibres were measured using the image analysis software ImageJ 1.40G (http://rsb.info.nih.gov/ij/download.html). The SEM images of at least 20 randomly selected samples were analysed to obtain diameter distribution histograms.

AUTHOR CONTRIBUTIONS

Jian Lu and Pengchao Liu conceived and designed this work. Pengchao Liu conducted the fabrication, measurements, and analysis with the help of Chengshengze Chu. Pengchao Liu and Chen Peng drafted and revised the manuscript. Ben Zhong Tang instructed the research of 4D-printed PLA-AIE chemosensors. Jian Lu revised the manuscript and supervised the project. All authors contributed to the experimentation and discussion.

ACKNOWLEDGEMENTS

The authors acknowledge the financial support provided by the Shenzhen-Hong Kong Science and Technology Innovation Cooperation Zone Shenzhen Park Project HZQB-KCZYB-2020030, Hong Kong RGC Theme-based Research Scheme (Project No: AoE/M-402/20), and the Shenzhen Science and Technology Program JCYJ20220818101204010.

CONFLICT OF INTEREST STATEMENT

The authors declare no conflict of interests.

DATA AVAILABILITY STATEMENT

The data that support the findings of this study are available from the corresponding author upon reasonable request.

ORCID

Zheng Zhao https://orcid.org/0000-0002-5536-0439
Xinyuan He https://orcid.org/0000-0002-4876-1656
Chen Peng https://orcid.org/0000-0002-7568-5409

REFERENCES

1. X. Shi, Y. Zuo, P. Zhai, J. Shen, Y. Yang, Z. Gao, M. Liao, J. Wu, J. Wang, X. Xu, *Nature* **2021**, *591*, 240.
2. J. Guo, B. Zhou, C. Yang, Q. Dai, L. Kong, *Adv. Funct. Mater.* **2019**, *29*, 1902898.
3. J.-H. Pu, X. Zhao, X.J. Zha, L. Bai, K. Ke, R.Y. Bao, Z.Y. Liu, M.-B. Yang, W. Yang, *J. Mater. Chem. A* **2019**, *7*, 15913.
4. S.-M. Jeong, J. Ahn, Y. K. Choi, T. Lim, K. Seo, T. Hong, G. H. Choi, H. Kim, B. W. Lee, S. Y. Park, *NPG Asia Mater.* **2020**, *12*, 32.
5. M. Liao, C. Wang, Y. Hong, Y. Zhang, X. Cheng, H. Sun, X. Huang, L. Ye, J. Wu, X. Shi, *Nat. Nanotechnol.* **2022**, *17*, 372.
6. J. He, C. Lu, H. Jiang, F. Han, X. Shi, J. Wu, L. Wang, T. Chen, J. Wang, Y. Zhang, *Nature* **2021**, *597*, 57.
7. W. Zeng, L. Shu, Q. Li, S. Chen, F. Wang, X. M. Tao, *Adv. Mater.* **2014**, *26*, 5310.
8. W. Tian, P. Song, H. Zhang, X. Duan, Y. Wei, H. Wang, S. Wang, *Prog. Mater. Sci.* **2023**, *132*, 101035.
9. A. D. Vethaak, J. Legler, *Science* **2021**, *371*, 672.
10. Z. Li, C. Feng, Y. Wu, X. Guo, *J. Hazard. Mater.* **2020**, *392*, 122418.
11. H. A. Leslie, M. J. M. van Velzen, S. H. Brandsma, A. D. Vethaak, J. J. Garcia-Vallejo, M. H. Lamoree, *Environ. Int.* **2022**, *163*, 107199.
12. J. Tang, W. Bu, W. Hu, Z. Zhao, L. Liu, C. Luo, R. Wang, S. Fan, S. Yu, Q. Wu, *ACS Nano* **2023**, *17*, 2440.
13. G. Rajeshkumar, S. Arvindh Seshadri, G. L. Devnani, M. R. Sanjay, S. Siengchin, J. Prakash Maran, N. A. Al-Dhabi, P. Karuppiah, V. A. Mariadhas, N. Sivarajasekar, A. Ronaldo Anuf, *J. Clean. Prod.* **2021**, *310*, 127483.
14. Y. Gao, J. Zhang, N. Cheng, Z. Liu, Y.-B. Wu, Q.-Q. Zhou, C.-Y. Li, M. Yu, S. Ramakrishna, R. Wang, *Nano Res.* **2023**, *16*, 810.
15. X. Li, C. Chu, L. Zhou, J. Bai, C. Guo, F. Xue, P. Lin, P. K. Chu, *Compos. Sci. Technol.* **2017**, *142*, 180.
16. W. Wang, B. Zhang, M. Li, J. Li, C. Zhang, Y. Han, L. Wang, K. Wang, C. Zhou, L. Liu, *Compos. B. Eng.* **2021**, *224*, 109192.
17. M. K. Mitchell, Hirt, D. E. *Polym. Eng. Sci.* **2015**, *55*, 1652.
18. D. Rasselet, A. Ruellan, A. Guinault, G. Miquelard-Garnier, C. Sollogoub, B. Fayolle, *Eur. Polym. J.* **2014**, *50*, 109.
19. N. Hegyesi, Y. Zhang, A. Kohári, P. Polyák, X. Sui, B. Pukánszky, *Ind. Crops Prod.* **2019**, *141*, 111799.
20. N. F. Zaaba, J. Mariatti. *Polym. Eng. Sci.* **2020**, *60*, 2061.
21. K. C. Hung, Y. L. Chen, J. H. Wu, *Polym. Degrad. Stab.* **2012**, *97*, 1680.
22. S. Gong, B. Zhang, J. Zhang, Z. L. Wang, K. Ren, *Adv. Funct. Mater.* **2020**, *30*, 1908724.
23. Y. Liu, G. Dzidotor, T. T. Le, T. Vinikoor, K. Morgan, E. J. Curry, R. Das, A. McClinton, E. Eisenberg, L. N. Apuzzo, *Sci. Transl. Med.* **2022**, *14*, eabi7282.
24. S. Khan, K. Joshi, S. Deshmukh, *Mater. Today: Proc*. **2022**, *50*, 2119.
25. P. Mieszczanek, T. M. Robinson, P. D. Dalton, D. W. Hutmacher, *Adv. Mater.* **2021**, *33*, 2100519.
26. T. M. Robinson, D. W. Hutmacher, P. D. Dalton, *Adv. Funct. Mater.* **2019**, *29*, 1904664.
27. T. D. Brown, P. D. Dalton, D. W. Hutmacher, *Adv. Mater.* **2011**, *23*, 5651.
28. R. Sanchez Diaz, J.-R. Park, L. L. Rodrigues, P. D. Dalton, E. M. De-Juan-Pardo, T. R. Dargaville, *Adv. Mater. Technol.* **2022**, *7*, 2100508.
29. M. Shahverdi, S. Seifi, A. Akbari, K. Mohammadi, A. Shamloo, M. R. Movahhedy, *Sci. Rep.* **2022**, *12*, 19935.
30. J. Meng, F. Boschetto, S. Yagi, E. Marin, T. Adachi, X. Chen, G. Pezzotti, S. Sakurai, S. Sasaki, T. Aoki, *Biomater. Adv.* **2022**, *135*, 112686.
31. T. D. Brown, P. D. Dalton, D. W. Hutmacher, *Prog. Polym. Sci.* **2016**, *56*, 116.
32. A. Hrynevich, I. Liashenko, P. D. Dalton, *Adv. Mater. Technol.* **2020**, *5*, 2000772.
33. I. Liashenko, A. Hrynevich, P. D. Dalton, *Adv. Mater.* **2020**, *32*, 2001874.
34. J. Luo, Z. Xie, J. W. Y. Lam, L. Cheng, H. Chen, C. Qiu, H. S. Kwok, X. Zhan, Y. Liu, D. Zhu, B. Z. Tang, *Chem. Commun.* **2001**, *18*, 1740.
35. V. Kachwal, J. C. Tan, *Adv. Sci.* **2022**, *10*, 2204848.
36. Y. Jiang, Y. Cheng, S. Liu, H. Zhang, X. Zheng, M. Chen, M. Khorloo, H. Xiang, B. Z. Tang, M. Zhu, *Natl. Sci. Rev.* **2021**, *8*, nwaa135.
37. Z. Li, X. Ji, H. Xie, B. Z. Tang, *Adv. Mater.* **2021**, *33*, 2100021.
38. Z. Li, P. Liu, X. Ji, J. Gong, Y. Hu, W. Wu, X. Wang, H. Q. Peng, R. T. Kwok, J. W. Lam, *Adv. Mater.* **2020**, *32*, 1906493.
39. R. Hu, A. Qin, B. Z. Tang, *Prog. Polym. Sci.* **2020**, *100*, 101176.
40. D. Ding, K. Li, B. Liu, B. Z. Tang, *Acc. Chem. Res.* **2013**, *46*, 2441.
41. F. Würthner, *Angew. Chem. Int. Ed.* **2020**, *59*, 14192.
42. X. He, H. Xie, L. Hu, P. Liu, C. Xu, W. He, W. Du, S. Zhang, H. Xing, X. Liu, *Aggregate* **2022**, *4*, e239.
43. Z. Xie, J. Zhu, L. Zhang, *ACS Appl. Mater. Interfaces* **2021**, *13*, 9027.
44. J. Zhu, Q. Zhang, H. Chen, R. Zhang, L. Liu, J. Yu, *ACS Appl. Mater. Interfaces* **2020**, *12*, 43634.

SUPPORTING INFORMATION

Additional supporting information can be found online in the Supporting Information section at the end of this article.

How to cite this article: P. Liu, C. Chu, W. Qiu, L. Cheng, J. Gu, Z. Mao, Z. Zhao, X. He, G. Liu, C. Peng, K. Man, B. Z. Tang, J. Lu, *Aggregate* **2024**, *5*, e521. https://doi.org/10.1002/agt2.521